Compacton existence and spin-orbit density dependence in Bose-Einstein condensates

F. Kh. Abdullaev,[1] M. S. A. Hadi,[2] B. Umarov,[1] L. A. Taib,[2] and M. Salerno[3]

[1]*Physical-Technical Institute, Uzbekistan Academy of Sciences, Tashkent, Bodomzor yuli, 2-b, Uzbekistan*

[2]*Department of Computational and Theoretical Sciences, Kulliyyah of Science, International Islamic University Malaysia, 25200 Kuantan, Pahang, Malaysia*

[3]*Dipartimento di Fisica "E.R. Caianiello", CNISM and INFN - Gruppo Collegato di Salerno, Universitá di Salerno, Via Giovanni Paolo II, 84084 Fisciano (SA), Italy*

(Received 12 August 2022; accepted 4 April 2023; published 26 April 2023)

We demonstrate the existence of compactons matter waves in binary mixtures of Bose-Einstein condensates (BEC) trapped in deep optical lattices (OL) subjected to equal contributions of intraspecies Rashba and Dresselhaus spin-orbit coupling (SOC) under periodic time modulations of the intraspecies scattering length. We show that these modulations lead to a rescaling of the SOC parameters that involves the density imbalance of the two components. This gives rise to density dependent SOC parameters that strongly influence the existence and the stability of compacton matter waves. The stability of SOC-compactons is investigated both by linear stability analysis and by time integrations of the coupled Gross-Pitaevskii equations. We find that SOC restricts the parameter ranges for stable stationary SOC-compacton existence but, on the other side, it gives a more stringent signature of their occurrence. In particular, SOC-compactons should appear when the intraspecies interactions and the number of atoms in the two components are perfectly balanced (or close to being balanced for the metastable case). The possibility to use SOC-compactons as a tool for indirect measurements of the number of atoms and/or the intraspecies interactions is also suggested.

DOI: 10.1103/PhysRevE.107.044218

I. INTRODUCTION

Recently, theoretical and experimental investigations of Bose-Einstein condensates (BEC) based on Floquet engineering (FE) of the different parameters have been performed (see, for example, the review [1]). The FE usually involves linear optical lattices, periodically shaken in time either through frequency or amplitude [2,3], or nonlinear optical lattices in which FE is realized through the modulation of the interactions [4]. Periodic modulations of the scattering lengths can also be used to emulate synthetic dimensions and to create density-dependent gauge fields [5], this being a research area of rapidly growing interest connected with interesting physical phenomena, including pair superfluidity, exactly defect-free Mott insulator states [6], etc. In the case of BEC with modulated interactions in double-well potential, the investigation shows that the tunneling transition amplitude between two wells depends on the relative imbalance of the atomic population between wells. This phenomenon leads to the suppression of the tunneling between wells for specific values of the imbalance [7], a prediction that was recently experimentally confirmed in [8].

For Bose-Einstein condensates trapped in a deep optical lattice (OL) the phenomenon of tunneling suppression leads to the existence of a new form of localized matter waves, also called BEC compactons, in which the density is strictly localized on a compact domain without any exponential decay tail at the boundary [4]. BEC compactons can exist not only in ordinary (e.g., single component) BEC but also in binary BEC mixtures [9,10], as well as in multidimensional contexts [11]. In the case of a deep modulation of the potential, the problem can be reduced to the nonlinear lattice described by a discrete nonlinear Schrödinger (DNLS) model with modulated nonlinearity. In this case the maximum localization is achieved with one-site compactons, i.e., excitations in which all the matter remains localized in a single well of the OL.

In binary BEC mixtures, however, another type of coupling, besides the one induced by the two-body inter and intraspecies interactions, is also possible, namely the spin-orbit-coupling (SOC). BEC with spin-orbit coupling (SOC-BEC) is presently receiving a lot of attention as with the ultracold atoms variety of synthetic SOC, which can be engineered and controlled by external laser fields. The experimental realization of SOC-BEC for the case of binary mixtures was reported in [2,3], while nonlinear excitations of intra-SOC and inter-SOC, i.e., with the spatial derivative of the SOC term acting inside each species or between the species, respectively, were theoretically investigated in [12]. For SOC-BEC trapped in deep OL, the existence of strongly localized excitation in the form of discrete breathers was theoretically investigated in [13] and the SOC tunability induced by periodic time modulations of the Zeeman term was demonstrated in [14]. Recently, the nonlinearity management of the spin-orbit coupled BEC has been investigated in [15] where it has been shown that for slow time periodic modulations of the nonlinearity, resonances between the frequencies of the modulation and of the intrinsic nonlinear modes (solitons) can lead to the appearance of instability and stability tongues for the solitons.

We remark that only a few studies exist for the case of SOC-BEC in deep OL subjected to nonlinear management [2]. This case is rather interesting because, compared to previous studies, the presence of the SOC term may affect the compacton matter waves excitations found in absence of SOC [4,9,10]. In particular, the spatial derivative of the SOC term may interfere with the tunneling of atoms between adjacent wells, making it unclear whether SOC-compactons may still be possible

The aim of the present paper is to provide an answer to the above problem, i.e., we investigate the formation of binary matter-wave compactons in the presence of SOC. For this, we consider an intra-SOC-BEC mixture in a deep OL subjected to strong nonlinear management (SNM) consisting of time-periodic modulations of the inter-species scattering length. Using the averaging method, we show that the SNM induces a rescaling of the inter-well tunneling constant and of the SOC parameters that depend on the density imbalance between neighboring sites, thus making the conditions for the compacton existence and stability much more involved.

In particular, we show that the interplay between SOC and interwell tunneling produce a big effect on the stability of the compactons which appears very much reduced by the presence of SOC. This is true even for the case of a single site compacton for which the existence range is completely independent of SOC parameters. A detailed linear stability analysis shows that single site compactons are stable for a wide range of interwell tunneling when the SOC parameter is relatively small. The SOC range, however, can be made wider by increasing the Rabi frequency. This is also true for compactons localized on more than one site.

It is worth noting that the possibility to induce by means of SNM a local density imbalance dependence on the SOC parameters is a fact that exists independently of compactons. Recently, a density-dependent SOC was also introduced in ultracold Bose and Fermi gases in terms of interaction assisted Raman processes [16]. We remark that our approach is different from this, being completely independent of indirect Raman processes (the density dependence of the SOC in our case is only due to scattering length modulations).

The paper is organized as follows. In Sec. II, we introduce the model equations for the system and show in detail the averaging procedure to derive the effective equations that are valid in the limit of strong modulations of the interspecies scattering length. In Secs. III and IV we study the SOC-compacton stationary and existence conditions, respectively. In Sec. V we present numerical results for the cases of one, two, and three site compactons and investigate their stability both by linear analysis and by direct time integrations of the equations of motion. Finally, in Sec. VI the main results of this paper are briefly summarized.

II. MODEL EQUATIONS AND AVERAGING

As a model for a quasione-dimensional BEC mixture trapped in an OL in the presence of SOC, we consider the following coupled Gross-Pitaevskii equations (CGPE):

$$i\hbar\frac{\partial\Psi}{\partial t} = H\Psi \equiv [H_0 + H_{nl}]\Psi,$$
$$H_0 \equiv \frac{p_x^2}{2m} + \frac{\hbar\kappa}{m}p_x\sigma_z + V_{ol}(x) + \hbar\bar{\Omega}\sigma_x,$$
$$H_{nl} \equiv 2\hbar\omega\begin{pmatrix}\sum_j a_{1j}|\Psi_j|^2 & 0\\ 0 & \sum_j a_{j2}|\Psi_j|^2\end{pmatrix}, \quad (1)$$

where $\sigma_{x,z}$ are usual Pauli matrices and $\Psi = (\Psi_1, \Psi_2)^T$ denotes the two-component wave function normalized to the total number of atoms. This quasi-1D model can be derived from a more general three-dimensional setting by considering a trapping potential with the transversal frequency $\omega_\perp$ much larger than the longitudinal one, $\omega_\perp \gg \omega_\parallel$. The linear part, H_0, of the Hamiltonian H includes the kinetic energy $p_x^2/(2m)$ of the condensate, the diagonal SOC term of strength κ, the off-diagonal Rabi oscillation term of frequency $\bar{\Omega}$, and an optical lattice in the x direction represented by a periodic potential $V_{ol}(x) \sim \sin^2(k_L x)$ where k_L is the lattice wave number. Note that the SOC term is diagonal in the two components, meaning that we are considering the intra-SOC case (a similar analysis can be done for the inter-SOC case with an off-diagonal κ term and a diagonal Zeeman term). The nonlinear part, H_{nl}, includes contact interactions, with a_{jj} $(j = 1, 2)$ and $a_{12,}$ the two-body intraspecies and interspecies scattering lengths, respectively. By rescaling variables and component wave functions according to:

$$x \to \frac{x}{k_L}, \quad t \to \omega_R t, \quad \text{where } \omega_R \equiv \frac{E_R}{\hbar} \equiv \frac{\hbar k_L^2}{2m};$$
$$V_{ol}(x) \to E_R V(x) = E_R V_0 \cos(2x),$$
$$\Psi_j \equiv \sqrt{\frac{\omega_R}{2\omega_\perp a_0}}\psi_j(x,t), \quad (2)$$

Eq. (1) can be put in the dimensionless form:

$$i\frac{\partial\psi_j}{\partial t} = \left[-\frac{\partial^2}{\partial x^2} + V(x) - (-1)^j i\frac{2\kappa}{k_L}\frac{\partial}{\partial x}\right]\psi_j + \left(\frac{a_{jj}}{a_0}|\psi_j|^2 + \frac{a_{j,3-j}}{a_0}|\psi_{3-j}|^2\right)\psi_j + \frac{\bar{\Omega}}{\omega_R}\psi_{3-j}, \quad (j = 1, 2) \quad (3)$$

with a_0 denoting the background scattering length and E_R the lattice recoil energy. By expanding the two component fields as $\psi_1(x,t) = \sum_n u_n(t)w(x-na)$ and $\psi_2(x,t) = \sum_n v_n(t)w(x-na)$ with $w(x-na)$ the lower band Wannier function of the underlying linear system [17], one obtains in the tight-binding approximation appropriate for deep optical lattices and the following discrete nonlinear Schrödinger system [13]:

$$\begin{aligned} iu_{n,t} =& -\Gamma(u_{n+1}+u_{n-1}) + i\sigma(u_{n+1}-u_{n-1}) \\ &+ \Omega v_n + [\gamma_1|u_n|^2 + \gamma|v_n|^2]u_n, \\ iv_{n,t} =& -\Gamma(v_{n+1}+v_{n-1}) - i\sigma(v_{n+1}-v_{n-1}) \\ &+ \Omega u_n + [\gamma|u_n|^2 + \gamma_2|v_n|^2]v_n. \end{aligned} \quad (4)$$

Here n denotes the lattice site at position na, a being the lattice constant, Γ is the intersite hopping coefficient, σ, Ω are the rescaled SOC strength and Rabi frequency, respectively, while γ_i, $i = 1, 2$ and γ are the coefficients of the intra and interspecies interactions, respectively. The system (4) is of

Hamiltonian form with the Hamiltonian given by

$$\begin{aligned} H = \sum_n \Big[&-\Gamma(u_{n+1}u_n^* + u_{n+1}^* u_n) \\ &- \Gamma(v_{n+1}v_n^* + v_{n+1}^* v_n) + i\sigma(u_{n+1}u_n^* - u_{n+1}^* u_n) \\ &- i\sigma(v_{n+1}v_n^* - v_{n+1}^* v_n) + \Omega(u_n v_n^* + u_n^* v_n) \\ &+ \frac{1}{2}(\gamma_1 |u_n|^4 + \gamma_2 |v_n|^4) + \gamma(t)|u_n|^2|v_n|^2 \Big]. \end{aligned} \tag{5}$$

In the absence of nonlinearity, i.e., $\gamma_1 = \gamma_2 = \gamma = 0$, the dispersion relation can be obtained by substituting $u_n = A\exp[i(kna - \mu t)]$ and $v_n = B\exp[i(kna - \mu t)]$ into Eq. (4), giving the following lower and upper branches for the chemical potentials of the two components:

$$\mu_\pm(k) = -2\Gamma\cos(k) \pm \sqrt{\Omega^2 + \sigma^2 \sin^2(k)}, \tag{6}$$

where we have fixed, here and below, $a = 1$ without any loss of generality. In the following we investigate the possibility of compacton formation via an interspecies NM, this being more simple than the intraspecies case since it involves the modulation of just a single parameter, i.e., the interspecies scattering length. Specifically, we keep the intraspecies nonlinear coefficients, γ_i, $i = 1, 2$, in Eq. (4) to be constants and assume the interspecies nonlinearity coefficient γ to be a time periodic function of the form:

$$\gamma(t) = \gamma^{(0)} + \frac{\gamma^{(1)}}{\epsilon}\cos\left(\frac{\omega t}{\epsilon}\right)$$

with ϵ a real parameter which allows to control the strength of the management and to separate the fast and slow time scales (see below). Our analysis will be valid in the limit of strong NM which requires $\epsilon \ll 1$. In this case it is possible to eliminate the explicit time dependence from Eq. (5) by means of the transformation:

$$u_n = U_n e^{-i\Lambda(\tau)|V_n|^2}, \quad v_n = V_n e^{-i\Lambda(\tau)|U_n|^2} \tag{7}$$

with

$$\Lambda(\tau) = \alpha\sin(\omega\tau), \quad \alpha = \frac{\gamma^{(1)}}{\omega}, \quad \tau = \frac{t}{\epsilon}, \tag{8}$$

and to apply the averaging method to eliminate the fast time scale. The resulting averaged equations for the amplitudes U_n and V_n are given in the Appendix [see Eqs. (A1) and (A2). It should be noted here that the averaged equations are only valid for $t \leqslant 1/\epsilon$ with accuracy of $\mathcal{O}(\epsilon)$ [18].

It turns out that the averaged equations also have Hamiltonian structure (see Appendix) with the same Hamiltonian (5) of the unmodulated system but with u_n and v_n replaced by U_n and V_n, respectively, and parameters Γ, σ, and Ω rescaled according to

$$\begin{aligned} \Gamma &\to \tilde{\Gamma}_i \equiv \Gamma J_0(\alpha\theta_{3-i}^+), \\ \sigma &\to \tilde{\sigma}_i \equiv \sigma J_0(\alpha\theta_{3-i}^+), \\ \Omega &\to \tilde{\Omega}_i \equiv \Omega J_0(\alpha\theta_0) \end{aligned} \tag{9}$$

with $i = 1, 2$, J_0 denoting the Bessel function of order zero and $\theta_1^\pm$, $\theta_2^\pm$, θ_0 defined as

$$\begin{aligned} \theta_0 &= |U_n|^2 - |V_n|^2, \\ \theta_1^\pm &= |U_{n\pm1}|^2 - |U_n|^2, \\ \theta_2^\pm &= |V_{n\pm1}|^2 - |V_n|^2. \end{aligned} \tag{10}$$

From this we see that the effect of the modulation is to introduce a dependence in the parameters Γ, σ of the unmodulated system, on the density imbalance between adjacent sites of the same component, and a dependence on the density imbalance between the two components on the same site, for Ω. Obviously the condition for compacton existence, i.e., the complete suppression of the tunneling at the compacton edges, also involves the SOC parameters and will have more restrictive conditions to be satisfied.

This can also be intuitively understood by observing that the term proportional to σ_z in the Hamiltonian changes the kinetic energy of both components while the term proportional to σ_x corresponds to Rabi-coupling leading to oscillations between the two BEC components. On the other hand, the variation of the kinetic energy due to the σ part of the SOC interferes with the natural dispersion of the system, i.e., with the intrawell tunneling Γ, while the Rabi term interferes with the stationarity condition of compacton. From this it is clear that the conditions of parameters for the SOC-compacton existence are expected to be more stringent than those in the absence of SOC.

Finally, we remark that while in the density-dependent SOC approach considered in Ref. [16], the rescaling of the parameter Ω involves both the zeroth and the first-order Bessel functions; in our case, due to the absence of indirect Raman processes, only the function J_0 is involved.

III. STATIONARY CONDITIONS FOR SOC-COMPACTONS

We look for stationary SOC-compactons of the form

$$U_n = A_n e^{-i\mu_1 t}, \quad V_n = B_n e^{-i\mu_2 t} \tag{11}$$

with A_n, B_n complex amplitudes and μ_1, μ_2 chemical potentials for the two BEC components. By substituting these expressions into the averaged equations for U_n, V_n given in the Appendix, one finds that all the time dependent exponential factors can be canceled out except the ones that are proportional to Ω, these being of the form

$$\begin{aligned} \Omega e^{-i(\mu_1+\mu_2)t}\{&\alpha A_n^2 B_n^* e^{2i\mu_2 t} J_1(\alpha\theta_0) - e^{2i\mu_1 t} B_n [J_0(\alpha\theta_0) \\ &- \alpha|A_n|^2 J_1(\alpha\theta_0)]\} \end{aligned} \tag{12}$$

for Eq. (A3), and similar expression but with the exchanges $A \leftrightarrow B$, $\mu_1 \leftrightarrow \mu_2$, and with a minus sign in front of J_0. From these expressions it is clear that stationary SOC-compactons are possible only if $\Omega = 0$ or if the chemical potentials of the two species are equal, i.e., $\mu_1 = \mu_2 \equiv \mu$. The corresponding steady-state equations then are

$$\mu_1 A_n = F_1|_{\Omega=0}, \quad \mu_2 B_n = F_2|_{\Omega=0} \tag{13}$$

for case $\Omega = 0$, and

$$\mu A_n = F_1, \quad \mu B_n = F_2 \tag{14}$$

for case $\mu_1 = \mu_2 = \mu$. Here F_1 and F_2 denote the right hand side of Eqs. (A3) and (A4), respectively, but with the replacements $U_n \to A_n$, $V_n \to B_n$. We remark that although the above stationary conditions are specific of the intra-SOC system, similar conditions would also appear for the inter-SOC system [19].

As we shall see in the next section, the condition $\Omega = 0$ is too restrictive and can be satisfied only for one-site compactons. In this case, however, although the stability of the solutions will be influenced by the SOC, the analytical expression of the solutions will be the same as for the non-SOC case.

Note that Eq. (14) implies the equality of the number of atoms N_1, N_2 in the two components, this being true in general also for multisite SOC-compactons. This can be easily understood from the fact that for $N_1 \neq N_2$ and $\Omega \neq 0$, there will be oscillations in the number of atoms that will make the zero tunneling conditions at the compacton edges impossible to satisfy. The only way to avoid this is to equilibrate the two components. This, however, requires the additional restriction of the equality of the intraspecies interactions (see below).

IV. EXISTENCE CONDITIONS FOR SOC-COMPACTONS

The conditions for the existence of stationary compactons are obtained once the following compacton ansatz is adopted:

$$\begin{aligned} &A_n, B_n \neq 0 \quad \text{if } n_0 \leqslant n \leqslant n_0 + s, \\ &A_n, B_n = 0 \quad \text{otherwise}, \end{aligned} \tag{15}$$

with n_0 and $n_0 + s$ denoting the left and right edges of the compacton, respectively, and s its width. Since the coupling in the stationary equations involves only first next neighbors, the substitution of the ansatz (15) into either Eq. (13) or Eq. (14) will give $2(s + 3)$ nontrivial equations in correspondence of sites $n_0 - 1, \dots, n_0 + s + 1$ and with all other equations, for $n \leqslant n_0 - 2$ and $n \geqslant n_0 + s + 2$, automatically satisfied. The compacton existence relies on the possibility to solve these $2(s + 3)$ equations for the nonzero amplitudes by achieving both the tunneling suppression at the compacton edges and the fixing of the chemical potentials.

A. One-site SOC-compactons

For a one-site compacton the condition $\Omega = 0$ implies existence conditions are completely independent of the SOC parameters σ, Ω and therefore will be similar to the case of BEC mixtures in absence of SOC considered in previous papers [9,10]. On the other hand, for $N_1 = N_2 = N/2$ the compacton existence will depend on Ω but not on σ; this is because the σ term always involves as a factor a zero amplitude on a site $n_0 \pm 1$ different to the site n_0. In both cases, however, the SOC terms will strongly influence the stability, therefore it is worth considering in more detail the existence conditions for these two cases.

Case $\mathbf{\Omega = 0}$. We take $s = 0$ in Eq. (15) and fix the amplitudes at site n_0 as $A_{n_0} = a + ib$, $B_{n_0} = c + id$, with a, b, c, d reals. By substituting into Eq. (13), one obtains, in correspondence to sites $n_0 \pm 1$, four equations that are automatically satisfied if $J_0(\alpha(c^2 + d^2)) = 0$ and $J_0(\alpha(a^2 + b^2)) = 0$, e.g., if a, b, c, d are taken as

$$a^2 + b^2 = N_1 = \frac{\xi_m}{\alpha}, \quad c^2 + d^2 = N_2 = \frac{\xi_l}{\alpha} \tag{16}$$

with ξ_m, ξ_l two different zeros of the Bessel function J_0. One can then check that the other two equations, e.g., the ones for the site n_0, give the chemical potentials as

$$\mu_1 = N_2\gamma^{(0)} + N_1\gamma_1, \quad \mu_2 = N_1\gamma^{(0)} + N_2\gamma_2. \tag{17}$$

Case $\mathbf{\Omega \neq 0}$. In this case, we must have $N_1 = N_2 = N/2$, so we fix $s = 0$ in Eq. (15) and take $A_{n_0} = B_{n_0} = a + ib$, with a, b reals. One can check that the equations in correspondence to the edges $n_0 \pm 1$ are automatically satisfied if $J_0(\alpha(a^2 + b^2)) = 0$, e.g., if $a^2 + b^2 = N/2 = \xi_l/\alpha$, with ξ_l a zero of J_0. The other two equations for the site n_0 can be solved for the chemical potential only if $\gamma_1 = \gamma_2 \equiv \tilde{\gamma}$, thus giving

$$\mu = \frac{N}{2}(\gamma^{(0)} + \tilde{\gamma}) + \Omega. \tag{18}$$

Note that in this case Ω enters the μ expressions simply as a shift.

B. Two-site SOC-compactons

For a two-site compacton, $\Omega = 0$ will not provide real solutions for the chemical potentials due to the presence of imaginary terms proportional to σ. It is possible, however, to eliminate such terms by considering some suitable ansatzes for the amplitudes. For this, let us fix $s = 1$ in Eq. (15) and take $A_{n_0} = B_{n_0+1} = a + ib$, $B_{n_0} = A_{n_0+1} = a - ib$, with a, b reals (*in-phase* solution). From Eq. (14) one then obtains eight equations in correspondence of sites $n_0 - 1, n_0, n_0 + 1,$ and $n_0 + 2$. One can show that these equations lead to the following solution for the chemical potential:

$$\mu = (a^2 + b^2)\left(\frac{\Omega - \Gamma}{a^2 - b^2} + \gamma + \gamma^{(0)}\right) \tag{19}$$

with a, b given by

$$\begin{aligned} a^2 &= \frac{\xi_l}{2\alpha}\left(1 + \frac{\Omega - \Gamma}{\sqrt{(\Gamma - \Omega)^2 + \sigma^2}}\right), \\ b^2 &= \frac{\xi_l}{2\alpha}\left(1 - \frac{\Omega - \Gamma}{\sqrt{(\Gamma - \Omega)^2 + \sigma^2}}\right), \end{aligned} \tag{20}$$

and ξ_l denoting a zero of J_0. Using Eq. (20) one can rewrite Eq. (19) in a more explicit form:

$$\mu = \frac{N}{4}(\gamma + \gamma^{(0)}) + \sqrt{\sigma^2 + (\Gamma - \Omega)^2}, \tag{21}$$

showing the full dependence on parameters Γ, σ, Ω and on the total numbers of atoms N.

Similarly, one can obtain *out-of-phase* two-site compactons solutions by assuming the ansatz $A_{n_0} = -B_{n_0+1} = a + ib$, $B_{n_0} = -A_{n_0+1} = a - ib$. In this case, the expressions for μ, a, b are the same as in Eqs. (19)–(21), except for the

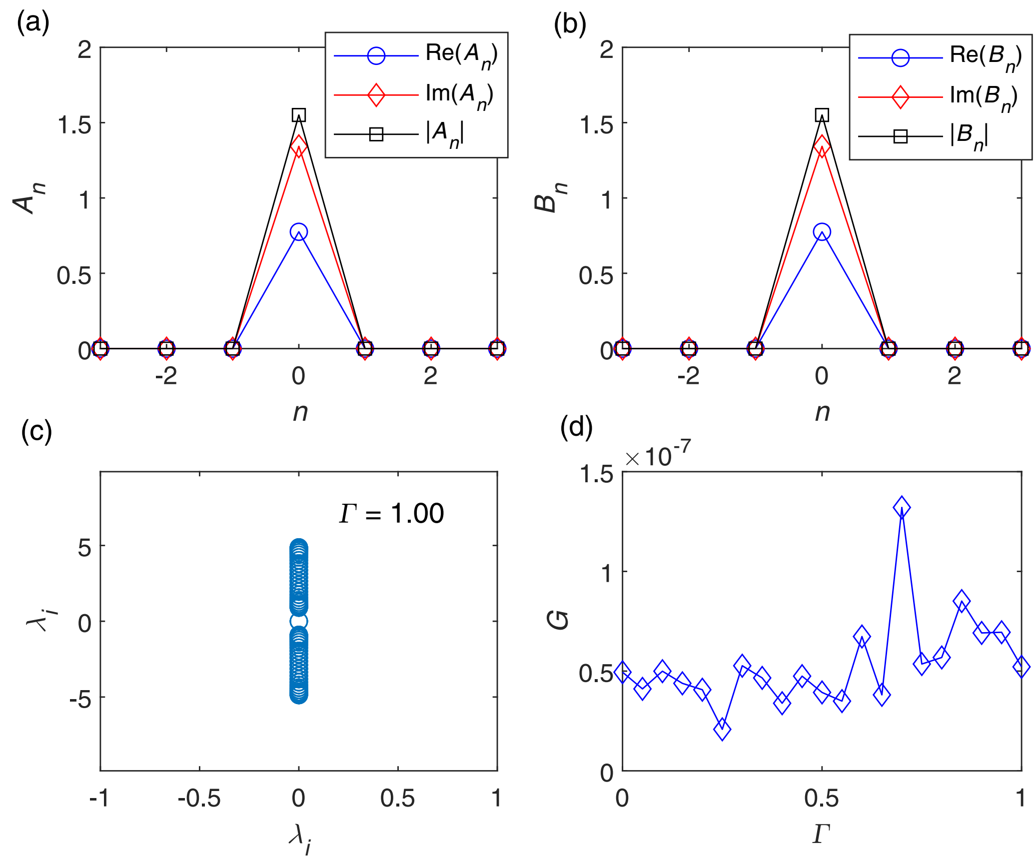

FIG. 1. (a), (b) Binary one-site compactons (14) localized at $n = 0$, for the case $\sigma = 0, \Omega = 0$, and with $A_0 = B_0 = a + ib$, where $a = 0.5\sqrt{\xi_1/\alpha}$ and $b = \sqrt{\xi_1/\alpha - a^2}$. Other parameters are fixed as $\Gamma = 1, \gamma_1 = \gamma_2 = -1, \gamma^{(0)} = -0.2, \gamma^{(1)} = 1.0, \omega = 1.0$. (c) The eigenvalue spectrum at $\Gamma = 1$, (d) gain G versus Γ.

replacement $\Gamma \to -\Gamma$ in all equations and for the change of sign in front of the fractions appearing inside the parentheses in Eq. (20).

C. Multi-site SOC-compactons

In principle, the above analysis, being completely general, can be applied to SOC-compactons of arbitrary size. The equations to solve, however, in these cases become much more involved for an exact analysis and one must recourse to numerical methods. An example of this is given for a three-site compacton in the next section.

V. NUMERICAL RESULTS

In order to check the above results, we will use both linear stability analysis and direct numerical integrations of the original discrete CGPE equations in Eq. (4). For the linear stability analysis, the standard procedure is employed by considering the ansatz with perturbation of the form

$$U_n = [A_n + \varepsilon(a_n e^{-i\lambda t} + b_n e^{i\lambda^* t})]e^{-i\mu t},$$
$$V_n = [B_n + \varepsilon(c_n e^{-i\lambda t} + d_n e^{i\lambda^* t})]e^{-i\mu t}, \quad (22)$$

where $\lambda = \lambda_r + i\lambda_i$ denotes the linearization eigenvalue and $\varepsilon \ll 1$. Substituting Eq. (22) in Eqs. (A3) and (A4), and taking only the terms with $O(\varepsilon)$ (linear terms of ε), one obtains an eigenvalue problem for λ that can be solved numerically. Ideally, the perturbation part in Eq. (22) will remain small (stable) if all imaginary eigenvalues λ_i are zeros or negligibly small, for gain $G = \max(|\lambda_i|) \simeq 0$.

Typically, the results of the linear stability analysis of SOC-compactons are further checked by direct integrations of both the averaged and original equations Eq. (4). Since they are found in agreement, however, results in the following will be reported only for the original equations.

A. One-site SOC-compactons

As discussed above, the existence condition for one-site SOC-compactons, apart from possible shifts of the chemical potential by Ω, are the same as in the absence of SOC. This, however, does not imply that there is no effect of the SOC on compactons because both σ and Ω can strongly influence their stability.

We show this by comparing results of the linear stability analysis in the case of absence of SOC, i.e., $\sigma = 0$, $\Omega = 0$, (see Fig. 1) with the ones obtained in the presence of SOC (see Figs. 2 and 3). From Fig. 1 we see that the linear spectrum has a gain G that is practically zero for all $\Gamma \in [0, 1]$, meaning that the solutions are stable, a fact that is already known from previous results [10]. By taking $\sigma = 2$ and setting $\Omega = -1$, we find that the solution becomes unstable [see panels (a) and (b) of Fig. 2], however, by decreasing $\sigma = 1$ and setting $\Omega = -2$, the stability can be restored almost for the whole

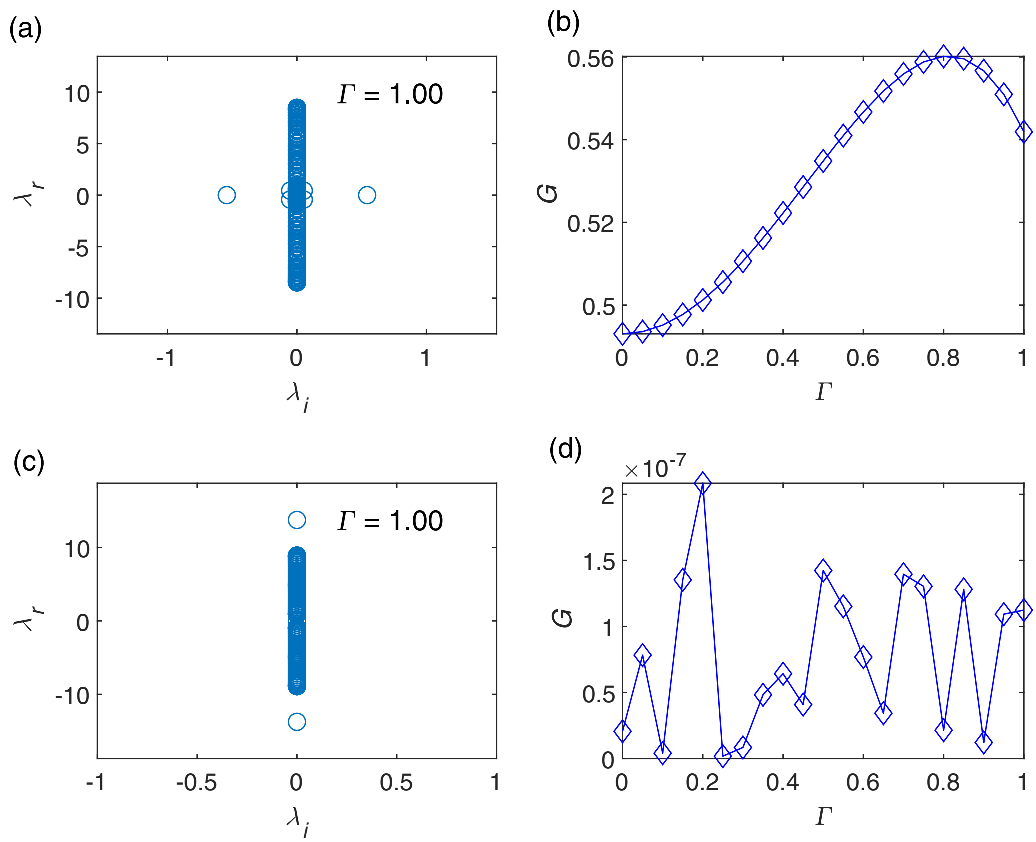

FIG. 2. Parameters for panels (a) and (b) are fixed as in panels (c) and (d) of Fig. 1 except $\sigma = 2$, $\Omega = -1$ and for panels (c) and (d), $\sigma = 1$, $\Omega = -2$.

range in Γ of the zero SOC case, as one can see from panels (c) and (d) of Fig. 2. Similar results are obtained for different choices of the system parameters and for different compacton amplitudes. In general, we have that stable one-site SOC-compactons can exist in wide regions of the parameter space.

We have also investigated the effects of the nonlinearity management parameters $\gamma^{(0)}$, $\gamma^{(1)}$ on the stability of one-site SOC-compactons. Note from Eq. (16) that the compacton amplitude is inversely proportional to the value of $\gamma^{(1)}$, despite $\gamma^{(1)}$ alone not affecting the stability. Remarkably, the solutions become significantly stable when $|\gamma^{(0)}|$ is much larger than $\gamma^{(1)}$, as demonstrated in Figs. 3(a) and 3(b), and oppositely, the solutions become unstable when $|\gamma^{(0)}|$ is much lower than $\gamma^{(1)}$, as portrayed in Figs. 3(c) and 3(d). The above linear stability results are further confirmed by nonlinear stability analysis achieved via numerical timeintegrations of the nonlinear system in Eq. (4), as one can see from Fig. 4.

B. Two-site SOC-compactons

For multisite compactons, we must necessarily have the condition $\Omega \neq 0$, i.e., equal chemical potentials for the two BEC components and this implies equal intraspecies interactions. Let us consider first the case of an in-phase SOC-compacton with amplitudes $A_0 = B_1 = a + ib$ and $A_1 = B_0 = a - ib$ with $a = \sqrt{\xi_1/2\alpha}$ and $b = \sqrt{\xi_1/\alpha - a^2}$. We fix parameters as follows: $\gamma_1 = \gamma_2 = 1$, $\gamma^{(0)} = 4$, $\gamma^{(1)} = 1$, $\omega = 1$, $\Omega = 4$, and $\sigma = 1$. Note that all the nonlinear parameters here are positive, i.e., interactions are repulsive. In panels (a) and (b) of Fig. 5 we show the real and imaginary parts versus n of the first and second component A_n, B_n, respectively, of a two-site in-phase compacton, while in the bottom panels, (c) and (d), their stability analysis is reported as a function of the parameter Γ. From panel (d) it is clear that for Γ less than ≈ 0.3 the gain G is positive and the solution is unstable, while for all $\Gamma \geqslant 0.3$ the gain reduces to zero and the solution becomes stable. Panel (c) of the figure just shows the stability in terms of the linear eigenvalues at $\Gamma = 1$ from which we see that they are all real numbers.

Similarly, for an out-of-phase two-site compacton we fix the amplitudes as $A_0 = -B_1 = a + ib$ and $B_0 = -A_1 = a - ib$ with the same a, b of the previous case. Parameters are fixed as $\gamma_1 = \gamma_2 = -1$, $\gamma^{(0)} = -4$, $\gamma^{(1)} = 1$, $\omega = 1$, $\Omega = -4$, and $\sigma = 1$. Results are reported in Fig. 6, where panels (a) and (b) depict the solutions of typical out-of-phase profiles and panels (c) and (d) show the results from the stability analysis. Notice that despite the type of interactions changed from repulsive to attractive, the range of stability is the same as for the in-phase case. Thus, independently on the sign of the interaction, in the interval $0.3 \leqslant \Gamma \leqslant 1$ both the in-phase and the out-of phase compactons appear to be stable. This is quite interesting because it shows SOC-compacton bistability in contrast with usual inter-site breathers (i.e., localized out-of-phase solutions with tails), which are known to be unstable in discretized spin-orbit-coupled BEC in absence of SNM [12].

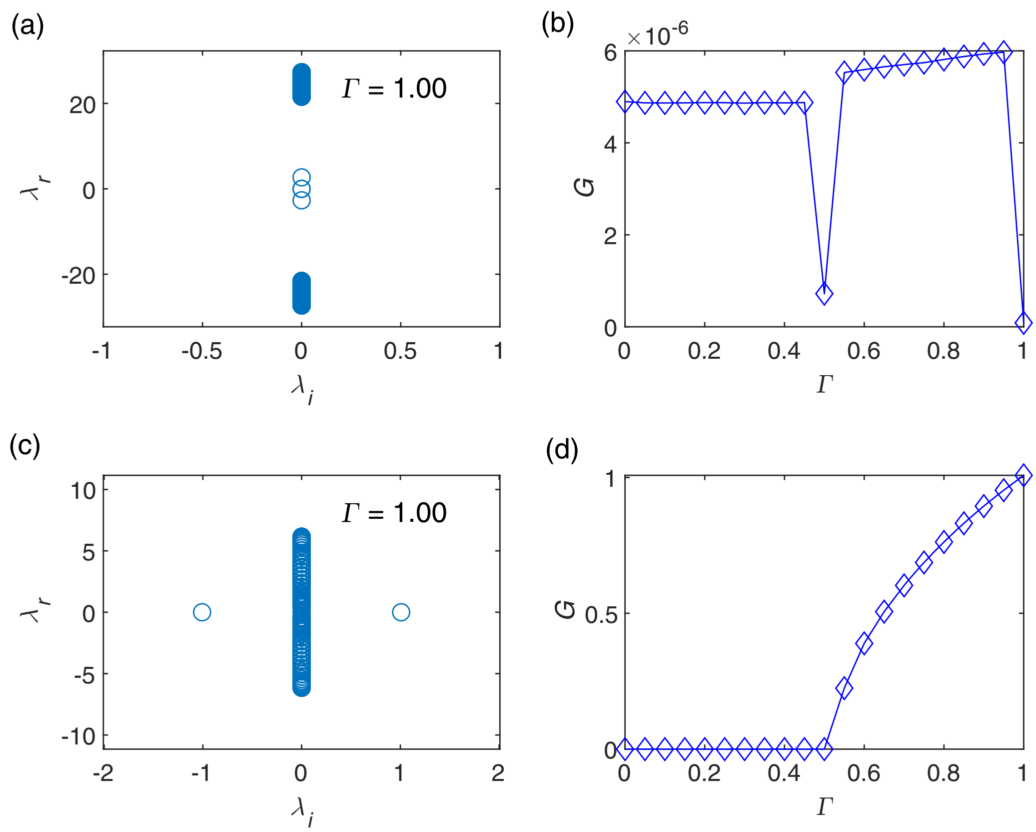

FIG. 3. Linear stability analysis for the one-site compactons; (a) The eigenvalue spectrum for case $\Gamma = 1, \gamma_1 = \gamma_2 = -1, \gamma^{(0)} = -1, \gamma^{(1)} = 0.2, \omega = 1.0, \Omega = -0.4, \sigma = 1$; (b) Gain G versus Γ with parameters as in (a), (c) The eigenvalue spectrum for case $\Gamma = 1, \gamma_1 = \gamma_2 = -1, \gamma^{(0)} = -0.2, \gamma^{(1)} = 1, \omega = 1, \Omega = -0.4, \sigma = 1$; (d) Gain G versus Γ with parameters as in (c).

The stability of the solution also depends on the ratio $\eta = |\gamma^{(0)}/\gamma^{(1)}|$ between the dc and ac strengths of the intersite interaction, with the two-site SOC-compacton becoming unstable for $\eta < 1$. This is shown in Fig. 7 for the case of the same two-site in-phase compacton depicted in Fig. 5 but with $\eta = 0.5$.

Finally, we find the results of the linear stability analysis to be in very good agreement with those obtained from direct numerical integrations of Eq. (4). An example of this is shown in Fig. 8 where the stable and unstable time evolution of the two-site in-phase compactons of Figs. 5 and 7 at $\Gamma = 1$, are reported.

C. Three-site SOC-compactons

Three-site SOC-compacton solutions are obtained from Eq. (15) with $s = 2$ by taking $\mu_1 = \mu_2 = \mu$ and assuming the following ansatz for the solution: $A_{n_0} = a + ib$, $B_{n_0} = a - ib$, $A_{n_0 \pm 1} = c + id$. and $B_{n_0 \pm 1} = c - id$ with a, b, c, d real numbers. Direct substitution of the ansatz into Eq. (14) provides ten equations which are reduced to six (for instance only those for sites $n_0 - 2, n_0 - 1, n_0$) thanks to the symmetry of the solution around the central site n_0. From the equations for the site $n_0 - 2$ one obtains the zero tunneling conditions for $A_{n_0 \pm 2}, B_{n_0 \pm 2}$ at the edges of the compacton in terms of roots of the Bessel function as in Eq. (16). Substituting these conditions into the equation relative to sites $n_0 - 1$, one obtains two equations that can be combined into the following expression for the chemical potential:

$$
\begin{aligned}
\mu = -\frac{1}{\mathrm{Re}(\omega_2)}\{&\alpha\Gamma[\mathrm{Re}(\omega_2\bar{z}_1 w_1) \\
&+ \mathrm{Re}(w_2 z_1 \bar{w}_1)] J_1(\alpha(|z_2|^2 - |w_2|^2)) \\
&+ \Gamma \mathrm{Re}(z_2) J_0(\alpha(|z_1|^2 - |w_1|^2)) \\
&- \Omega \mathrm{Re}(w_1) - \gamma |w_1|^2 \mathrm{Re}(w_2) \\
&- \gamma^{(0)} |w_1|^2 \mathrm{Re}(w_2) - \alpha\sigma J_1(\alpha(|z_2|^2 - |w_2|^2)) \\
&\cdot [\mathrm{Im}(w_2 \bar{z}_1 w_1) - \mathrm{Im}(w_2 z_1 \bar{w}_1)] \\
&- \sigma J_0(\alpha(|z_1|^2 - |w_1|^2)) \mathrm{Im}(z_2)\}.
\end{aligned} \tag{23}
$$

Here we used $\gamma_1 = \gamma_2 = \gamma$ and denoted $z_1 = a + ib$, $z_2 = a - ib$, $w_1 = c + id$, and $w_2 = c - id$. Lastly, from the equations for site n_0 one gets:

$$
\begin{aligned}
&\mu z_{j+1} + 2\alpha\Gamma z_{j+1}(\bar{w}_{2-j} z_{2-j} + w_{2-j}\bar{z}_{2-j}) \\
&\quad \cdot J_1(\alpha(|w_{j+1}|^2 - |z_{j+1}|^2)) \\
&\quad + \alpha\Omega\big(z_{2-j}|z_{j+1}|^2 + z_{2-j} z_{j+1}^2\big) \\
&\quad \cdot J_1(\alpha(|z_{j+1}|^2 - |z_{2-j}|^2)) \\
&\quad + 2\Gamma w_{j+1} J_0(\alpha(|w_{2-j}|^2 - |z_{2-j}|^2)) \\
&\quad - \Omega z_{2-j} J_0(\alpha(|z_{j+1}|^2 - |z_{2-j}|^2)) \\
&\quad - \gamma |z_{j+1}|^2 z_{j+1} - \gamma^{(0)} |z_{2-j}|^2 z_{j+1} = 0,
\end{aligned} \tag{24}
$$

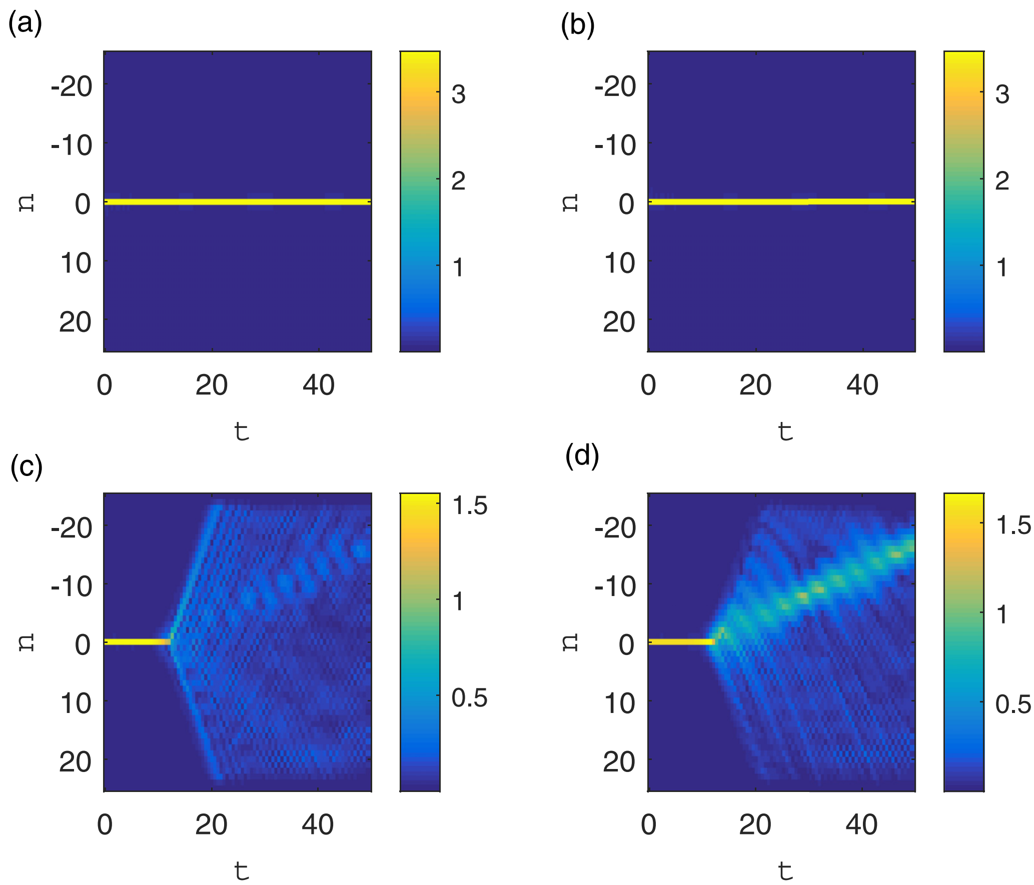

FIG. 4. Space-time evolution of the on-site compactons by solving Eq. (4) with $\epsilon = 0.01$, (a) $|u_n|$ and (b) $|v_n|$ for stable case as in Fig. 3(a) while (c) $|u_n|$ and (d) $|v_n|$ for unstable case as in Fig. 3(c).

with $j = 0, 1$. These nonlinear equations together with the previous ones should be solved numerically for a, b, c, d, giving the the compacton amplitudes of the two components at sites $n_0, n_0 \pm 1$.

Stability patterns for three-site compactons are in general similar to the ones previously investigated, as shown in Fig. 9, the only distinctive feature being the absence of stable solutions for the case $\gamma^{(0)} \leqslant \gamma^{(1)}$, and even for case $\gamma^{(0)} > \gamma^{(1)}$; if the difference is not sufficiently large, the solution might become unstable as depicted in Fig. 10. Lastly, in the top and bottom panels of Fig. 11 we report the time evolution obtained from numerical integrations of Eq. (4) by initial conditions the solutions at $\Gamma = 1$ depicted in Figs. 9 and 10, for which the linear stability analysis predicts stability and instability, respectively. As one can see from panels (a) and (b) and (c) and (d) of Fig. 11, these predictions are fully confirmed by direct numerical integrations of Eq. (4).

VI. CONCLUSIONS

In this paper we have investigated the existence and stability properties of compacton matter wave excitations of binary BEC mixtures with spin-orbit coupling trapped in an OL, subjected to SNM. We considered for simplicity an inter-SOC system (i.e., with an off-diagonal Rabi term) and assumed both the OL to be deep enough to justify the tight-binding approximation, and the strength and the frequency of the modulation to be large enough to use the averaging method.

Within this model, we derived effective averaged equations of motion for the matter wave complex amplitudes in the form of a two coupled discrete NLS and demonstrated that the SNM introduces a local density imbalance dependence not only in the tunneling parameter Γ but also in the SOC parameters σ and Ω. This density dependence of the SOC parameters persists in the system independently of the SOC-compacton existence.

The dependence of both σ and Ω on the local density imbalance, however, give rise to conditions for stable SOC-compactons existence that are more restrictive than the ones obtained in the absence of SOC. In general, the stationarity condition requires the equality of the chemical potentials of the two components, a fact that can be satisfied when the number of atoms of the two species are equal as well as their intraspecies nonlinearities. We have also investigated the stability of SOC-compactons versus the system parameters, i.e., the SOC strength σ, the Rabi frequency Ω, the coupling or hopping constant Γ, and the ratio between the nonlinear coefficients $\gamma^{(0)}, \gamma^{(1)}$. This has been done both using a linear stability analysis of the averaged equations and by direct numerical time integrations of the original nonlinear PDE equations. Numerical simulations show that by keeping the other parameters fixed, an enlargement of the stability region of SOC-compactons can be achieved by decreasing σ or by

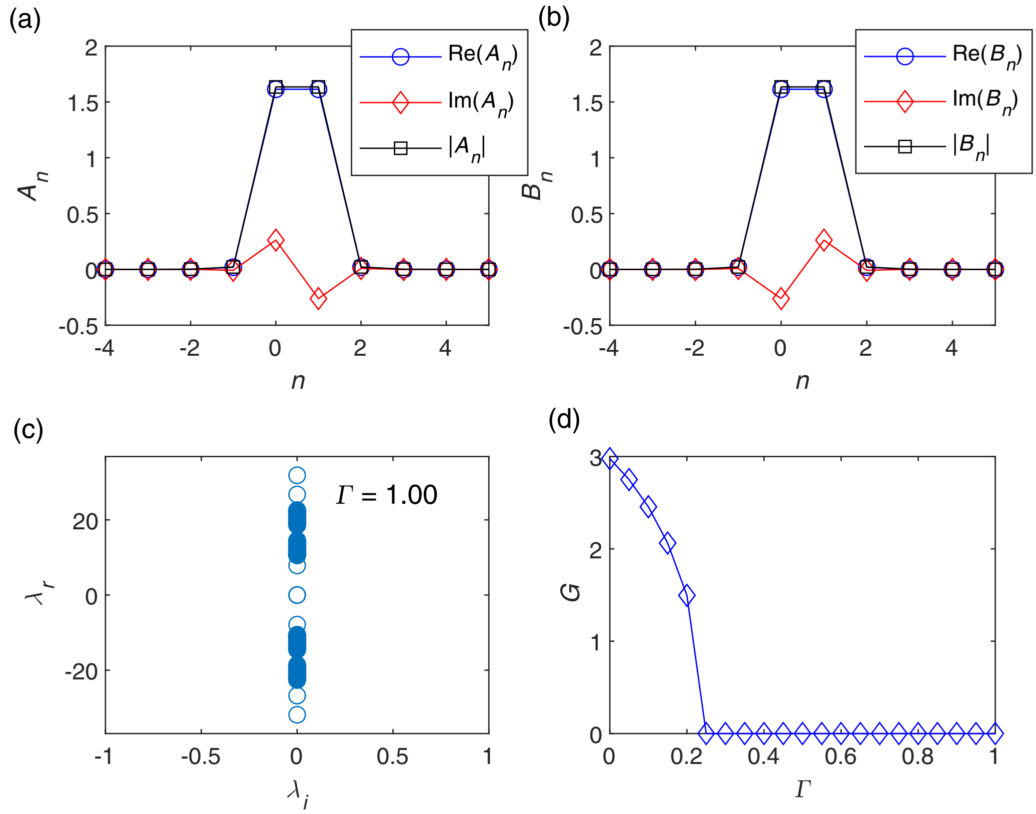

FIG. 5. Two-site in-phase compacton for case $\gamma_1 = \gamma_2 = 1$, $\gamma^{(0)} = 4$, $\gamma^{(1)} = 1$, $\omega = 1$, $\Omega = 4$, and $\sigma = 1$.

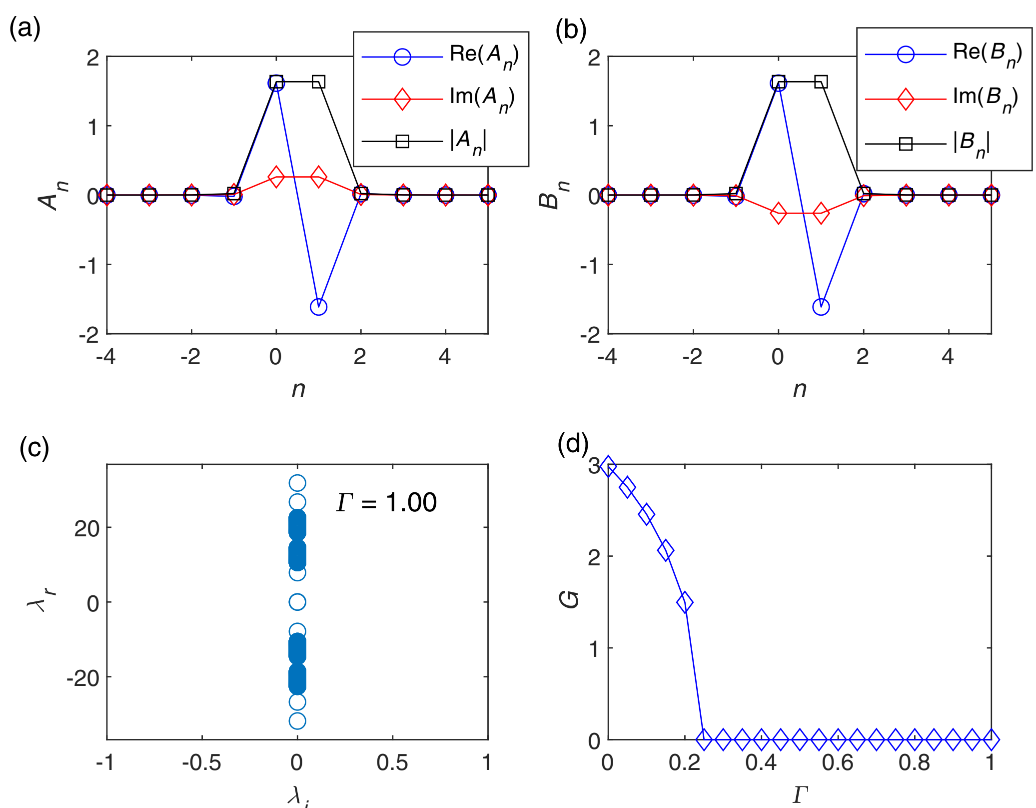

FIG. 6. Two-site out-phase compacton for case $\gamma_1 = \gamma_2 = -1$, $\gamma^{(0)} = -4$, $\gamma^{(1)} = 1$, $\omega = 1$, $\Omega = -4$, and $\sigma = 1$.

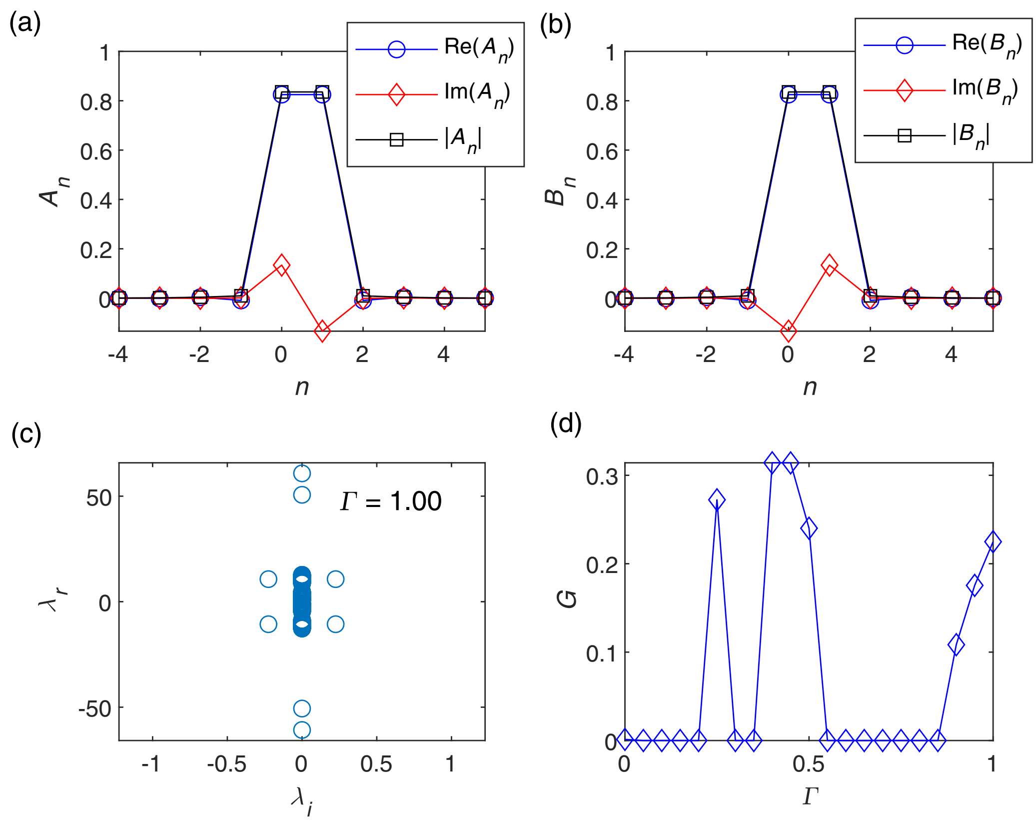

FIG. 7. Two-site in-phase compacton for case $\gamma_1 = \gamma_2 = 1$, $\gamma^{(0)} = 4$, $\gamma^{(1)} = 8.0$, $\omega = 1$, $\Omega = 4$, and $\sigma = 1$.

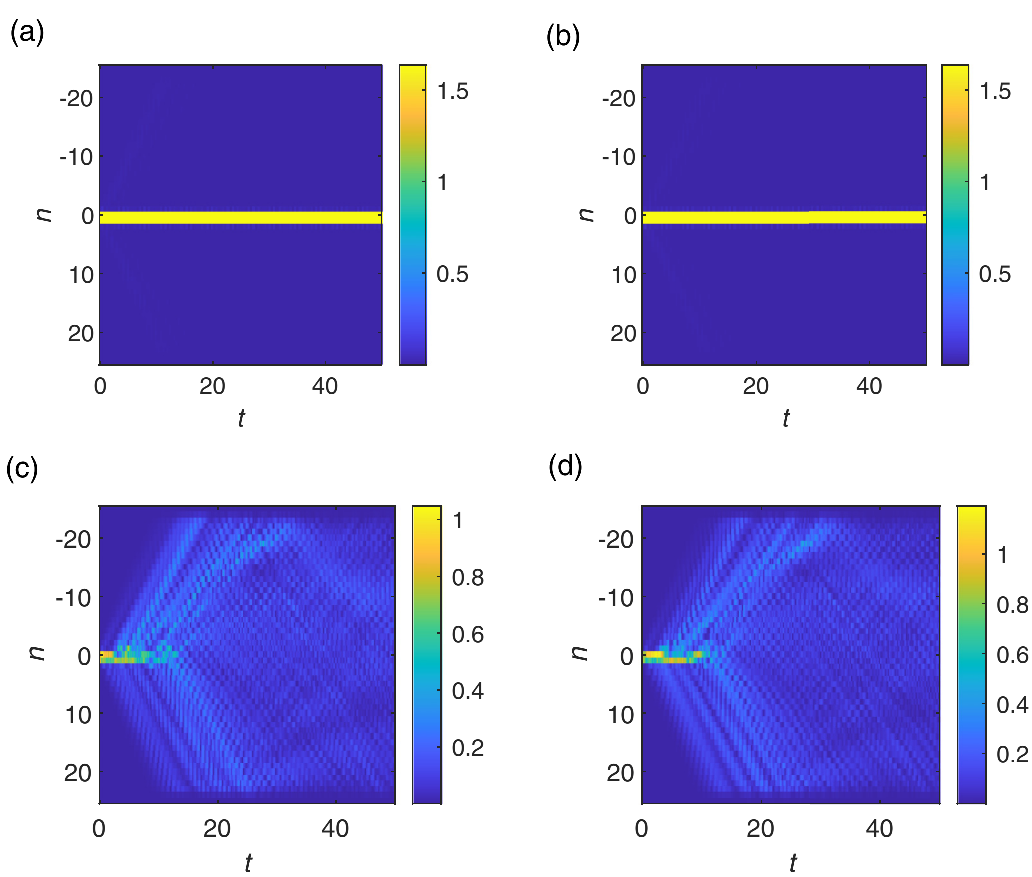

FIG. 8. Space-time evolution of the two-site compactons obtained from numerical integrations of Eq. (4) with $\epsilon = 0.01$. (a) $|u_n|$ and (b) $|v_n|$ for the stable case at $\Gamma = 1$ in Fig. 5. (c) $|u_n|$ and (d) $|v_n|$ for unstable case at $\Gamma = 1$ in Fig. 7.

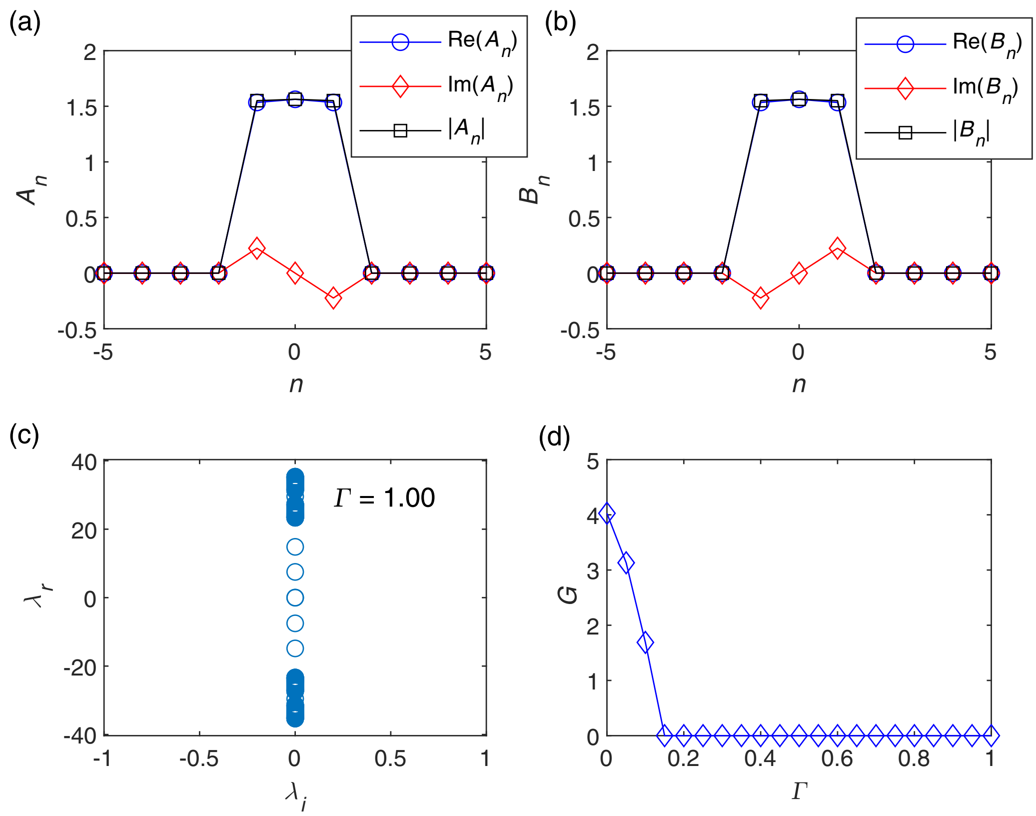

FIG. 9. Three-site compacton for case $\gamma_1 = \gamma_2 = 1$, $\gamma^{(0)} = 10$, $\gamma^{(1)} = 1$, $\omega = 1$, $\Omega = 4$, and $\sigma = 1$.

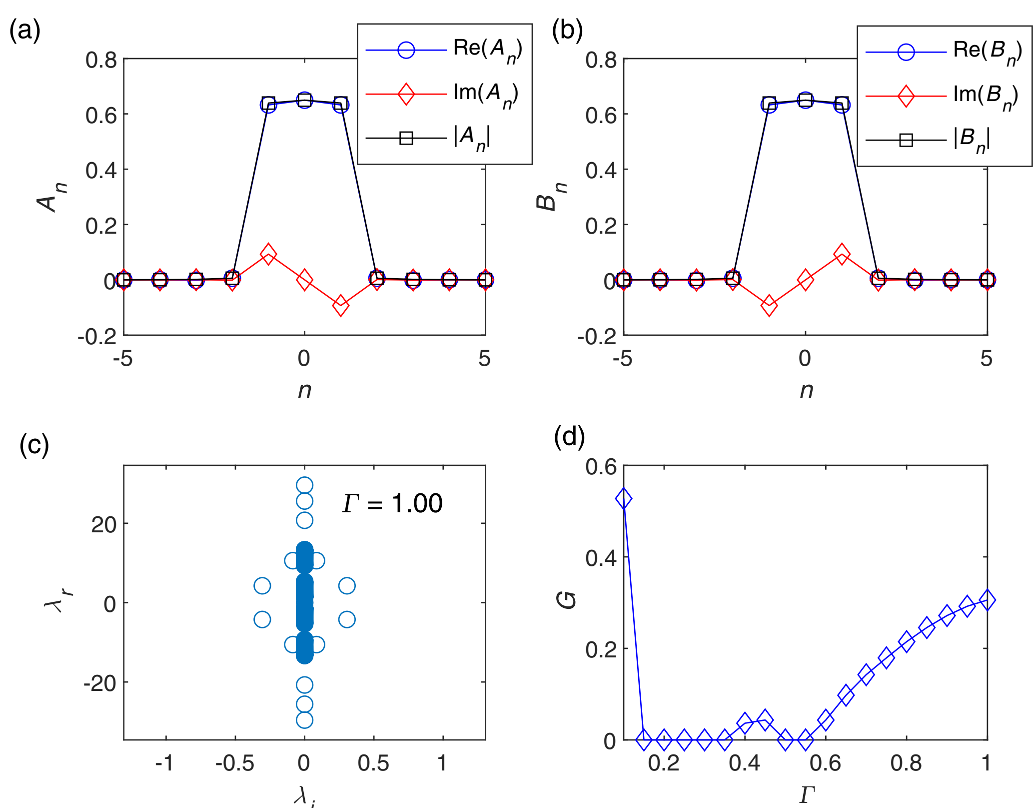

FIG. 10. Three-site compacton for case $\gamma_1 = \gamma_2 = 1$, $\gamma^{(0)} = 10$, $\gamma^{(1)} = 6.0$, $\omega = 1$, $\Omega = 4$, and $\sigma = 1$.

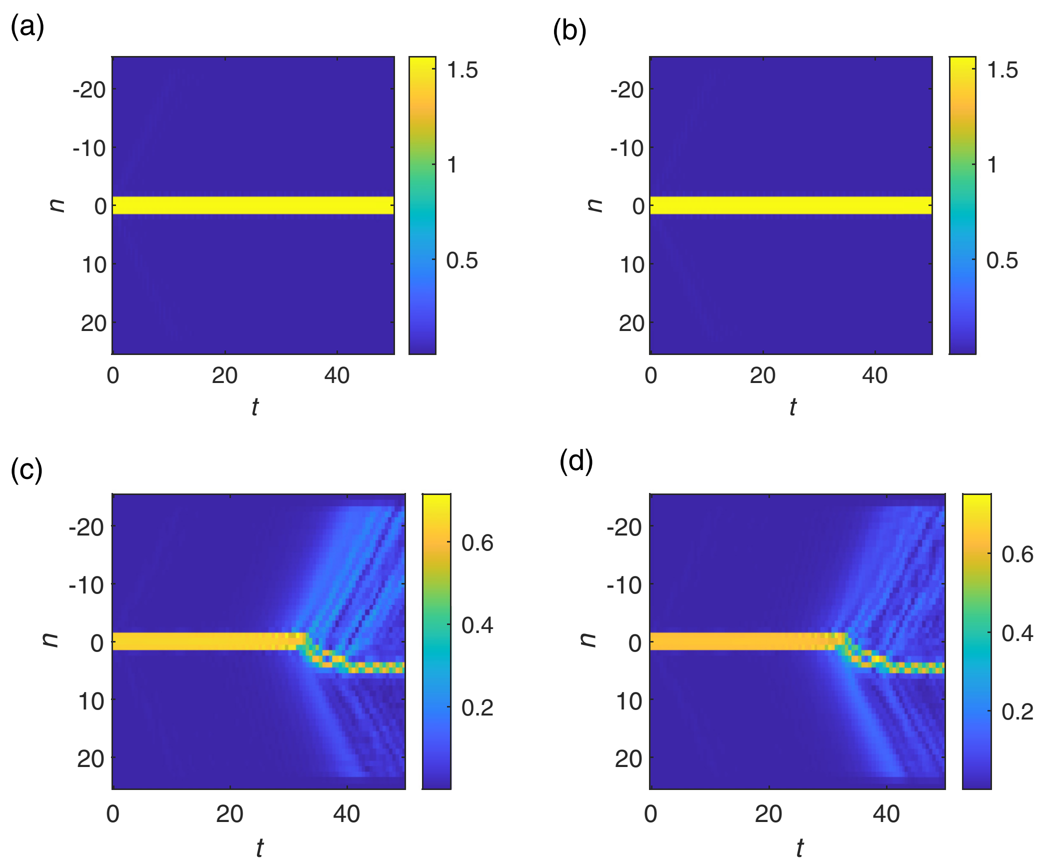

FIG. 11. Space-time evolution of the three-site compactons obtained from numerical integrations of Eq. (4) with $\epsilon = 0.01$, (a) $|u_n|$ and (b) $|v_n|$ for the stable case at $\Gamma = 1$ in Fig. 9. (c) $|u_n|$ and (d) $|v_n|$ for unstable case at $\Gamma = 1$ in Fig. 10.

increasing Ω. Stability also seems more easily obtainable for $|\gamma^{(0)}| > |\gamma^{(1)}|$ and large values of Γ.

From this, we conclude that while on one side the SOC restricts the parameter range for stationary SOC-compacton existence, on the other side it gives a more stringent signature of their occurrence. Indeed, they should appear when the intra-species interactions and the number of atoms in the two components are perfectly balanced (or close to being balanced for metastable cases). This suggests SOC-compactons as possible tools for indirect measurements of the number of atoms, and/or the intraspecies interactions in experiments.

ACKNOWLEDGMENTS

This research was supported by International Islamic University Malaysia (IIUM) and the Ministry of Higher Education (MOHE), Malaysia through Fundamental Research Grant Scheme (FRGS/1/2016/STG02/UIAM/02/1). M.S. acknowledges the IIUM in Kuantan for hospitality and for partial support.

APPENDIX: AVERAGED EQUATIONS AND HAMILTONIAN STRUCTURE

Below we provide the derivation of the averaged system Eq. (11). By substituting Eq. (7) into Eq. (4) we get:

$$\begin{aligned} iU_{n,t} =& -i\Gamma U_n(\langle\Lambda\bar{X}_1^+\rangle V_n - \langle\Lambda X_1^+\rangle V_n^*) \\ & - \sigma U_n(\langle\Lambda\bar{X}_1^-\rangle V_n + \langle\Lambda X_1^-\rangle V_n^*) \\ & + i\Omega\big(\langle\Lambda\bar{X}_0^+\rangle V_n|U_n|^2 - \langle\Lambda X_0^-\rangle V_n^* U_n^2\big) \\ & - \Gamma\langle X_2^+\rangle + i\sigma\langle X_2^-\rangle + \Omega\langle X_0^-\rangle V_n \\ & + \gamma_1|U_n|^2U_n + \gamma^{(0)}|V_n|^2U_n, \end{aligned} \tag{A1}$$

$$\begin{aligned} iV_{n,t} =& -i\Gamma V_n(\langle\Lambda\bar{X}_2^+\rangle U_n - \langle\Lambda X_2^+\rangle U_n^*) \\ & + \sigma V_n(\langle\Lambda\bar{X}_2^-\rangle U_n + \langle\Lambda X_2^-\rangle U_n^*) \\ & + i\Omega\big(\langle\Lambda\bar{X}_0^+\rangle U_n|V_n|^2 - \langle\Lambda X_0^-\rangle U_n^* V_n^2\big) \\ & - \Gamma\langle X_1^+\rangle - i\sigma\langle X_1^-\rangle + \Omega\langle X_0^+\rangle U_n \\ & + \gamma_2|V_n|^2V_n + \gamma^{(0)}|U_n|^2V_n, \end{aligned} \tag{A2}$$

where

$$\begin{aligned} X_2^\pm &= U_{n+1}e^{i\Lambda(|V_{n+1}|^2-|V_n|^2)} \pm U_{n-1}e^{i\Lambda(|V_{n-1}|^2-|V_n|^2)}, \\ X_1^\pm &= V_{n+1}e^{i\Lambda(|U_{n+1}|^2-|U_n|^2)} \pm V_{n-1}e^{i\Lambda(|U_{n-1}|^2-|U_n|^2)}, \\ X_0^\pm &= e^{\pm i\Lambda(|U_n|^2-|V_n|^2)}, \end{aligned}$$

and $\langle\cdot\rangle$ is the rapid modulated term to be averaged. The averaged terms can be evaluated as

$$\begin{aligned} \langle\Lambda X_1^\pm\rangle &= V_{n+1}\langle\Lambda e^{i\Lambda\theta_1^+}\rangle \pm V_{n-1}\langle\Lambda e^{i\Lambda\theta_1^-}\rangle, \\ \langle\Lambda X_2^\pm\rangle &= U_{n+1}\langle\Lambda e^{i\Lambda\theta_2^+}\rangle \pm U_{n-1}\langle\Lambda e^{i\Lambda\theta_2^-}\rangle, \\ \langle X_1^\pm\rangle &= V_{n+1}\langle e^{i\Lambda\theta_1^+}\rangle \pm V_{n-1}\langle e^{i\Lambda\theta_1^-}\rangle, \end{aligned}$$

$$\langle X_2^{\pm}\rangle = U_{n+1}\langle e^{i\Lambda\theta_2^+}\rangle \pm U_{n-1}\langle e^{i\Lambda\theta_2^-}\rangle,$$
$$\langle \Lambda X_0^{\pm}\rangle = \langle \Lambda e^{\pm i\Lambda\theta_0}\rangle, \quad \langle X_0^{\pm}\rangle = \langle e^{\pm i\Lambda\theta_0}\rangle$$

with

$$\langle \Lambda e^{\pm i\Lambda\theta_j^{\pm}}\rangle = \frac{\omega}{2\pi}\int_0^{2\pi/\omega}\frac{\gamma^{(1)}}{\omega}\sin(\omega\tau)e^{\pm i\frac{\gamma^{(1)}}{\omega}\theta_j^{\pm}\sin(\omega\tau)}\,d\tau$$
$$= \pm i\alpha J_1(\alpha\theta_j^{\pm}), \quad \langle e^{\pm i\Lambda\theta_j^{\pm}}\rangle = J_0(\alpha\theta_j^{\pm}),$$
$$\langle \Lambda e^{\pm i\Lambda\theta_0}\rangle = \pm i\alpha J_1(\alpha\theta_0), \quad \langle e^{\pm i\Lambda\theta_0}\rangle = J_1(\alpha\theta_0).$$

Here J_0, J_1 are the Bessel functions of orders 0 and 1, respectively, and $\alpha = \gamma^{(1)}/\omega$ and $\theta_1^{\pm}$, $\theta_2^{\pm}$, θ_0 are defined as in Eq. (10). Substituting the above averages into Eqs. (A1) and (A2) yields

$$\begin{aligned} iU_{n,t} = &-\Gamma\{\alpha U_n[(V_{n+1}^*V_n + V_{n+1}V_n^*)J_1(\alpha\theta_1^+)\\ &+(V_{n-1}^*V_n + V_{n-1}V_n^*)J_1(\alpha\theta_1^-)] + U_{n+1}J_0(\alpha\theta_2^+)\\ &+U_{n-1}J_0(\alpha\theta_2^-)\} + \{\gamma_1|U_n|^2 + \gamma^{(0)}|V_n|^2\}U_n\\ &+i\sigma\{\alpha U_n[(V_{n+1}^*V_n - V_{n+1}V_n^*)J_1(\alpha\theta_1^+) - (V_{n-1}^*V_n\\ &-V_{n-1}V_n^*)J_1(\alpha\theta_1^-)] + U_{n+1}J_0(\alpha\theta_2^+) - U_{n-1}J_0(\alpha\theta_2^-)\}\\ &-\Omega\big\{\alpha J_1(\alpha\theta_0)\big(V_n|U_n|^2 + V_n^*U_n^2\big) - V_nJ_0(\alpha\theta_0)\big\}, \end{aligned} \tag{A3}$$

$$\begin{aligned} iV_{n,t} = &-\Gamma\{\alpha V_n[(U_{n+1}^*U_n + U_{n+1}U_n^*)J_1(\alpha\theta_2^+)\\ &+(U_{n-1}^*U_n + U_{n-1}U_n^*)J_1(\alpha\theta_2^-)] + V_{n+1}J_0(\alpha\theta_1^+)\\ &+V_{n-1}J_0(\alpha\theta_1^-)\} + \{\gamma_2|V_n|^2 + \gamma^{(0)}|U_n|^2\}V_n\\ &-i\sigma\{\alpha V_n[(U_{n+1}^*U_n - U_{n+1}U_n^*)J_1(\alpha\theta_2^+) - (U_{n-1}^*U_n\\ &-U_{n-1}U_n^*)J_1(\alpha\theta_2^-)] + V_{n+1}J_0(\alpha\theta_1^+) - V_{n-1}J_0(\alpha\theta_1^-)\}\\ &+\Omega\big\{\alpha J_1(\alpha\theta_0)\big(U_n|V_n|^2 + U_n^*V_n^2\big) + U_nJ_0(\alpha\theta_0)\big\}. \end{aligned} \tag{A4}$$

Furthermore, Eqs. (A3) and (A4) can be written in terms of $iU_{n,t} = \delta H_{av}/\delta U_n^*$ and $iV_{n,t} = \delta H_{av}/\delta V_n^*$, respectively, where the averaged Hamiltonian is

$$\begin{aligned} H_{av} = \sum_n \Big[&-\Gamma J_0(\alpha\theta_2^+)(U_{n+1}U_n^* + U_{n+1}^*U_n)\\ &-\Gamma J_0(\alpha\theta_1^+)(V_{n+1}V_n^* + V_{n+1}^*V_n)\\ &+i\sigma J_0(\alpha\theta_2^+)(U_{n+1}U_n^* - U_{n+1}^*U_n)\\ &-i\sigma J_0(\alpha\theta_1^+)(V_{n+1}V_n^* - V_{n+1}^*V_n)\\ &+\Omega J_0(\alpha\theta_0)(U_nV_n^* + U_n^*V_n)\\ &+\frac{1}{2}(\gamma_1|U_n|^4 + \gamma_2|V_n|^2) + \gamma^{(0)}|U_n|^2|V_n|^2\Big]. \end{aligned} \tag{A5}$$

By comparing the averaged Hamiltonian in Eq. (A5) with the original Hamiltonian Eq. (5), their terms coincide if one rescales the tunneling or hopping constant Γ, the SOC parameter σ, and the Rabi frequency Ω according to Eq. (9).

[1] M. Bukov, L. D'Alessio, and A. Polkovnikov, Adv. Phys. **64**, 139 (2015).
[2] Y. J. Lin, K. Jiménez-García, and I. B. Spielman, Nature (London) **471**, 83 (2011).
[3] V. Galitski and I. B. Spielman, Nature (London) **494**, 49 (2013).
[4] F. Kh. Abdullaev, P. G. Kevrekidis, and M. Salerno, Phys. Rev. Lett. **105**, 113901 (2010).
[5] S. Greschner, G. Sun, D. Poletti, and L. Santos, Phys. Rev. Lett. **113**, 215303 (2014).
[6] Á. Rapp, X. Deng, and L. Santos, Phys. Rev. Lett. **109**, 203005 (2012).
[7] J. Gong, L. Morales-Molina, and P. Hänggi, Phys. Rev. Lett. **103**, 133002 (2009).
[8] F. Meinert, M. J. Mark, K. Lauber, A. J. Daley, and H.-C. Nägerl, Phys. Rev. Lett. **116**, 205301 (2016).
[9] F. Kh. Abdullaev, M. S. A. Hadi, M. Salerno, and B. Umarov, Phys. Rev. A **90**, 063637 (2014).
[10] F. Kh. Abdullaev, M. S. A. Hadi, M. Salerno, and B. Umarov, J. Phys. B: At. Mol. Opt. Phys. **50**, 165301 (2017).
[11] J. D'Ambroise, M. Salerno, P. G. Kevrekidis, and F. Kh. Abdullaev, Phys. Rev. A **92**, 053621 (2015).
[12] P. P. Beličev, G. Gligorić, J. Petrovic, A. Maluckov, L. Hadžievski, and B. A. Malomed, J. Phys. B: At. Mol. Opt. Phys. **48**, 065301 (2015).
[13] M. Salerno and F. K. Abdullaev, Phys. Lett. A **379**, 2252 (2015).
[14] M. Salerno, F. Kh. Abdullaev, A. Gammal, and L. Tomio, Phys. Rev. A **94**, 043602 (2016).
[15] S. Sakaguchi and B. A. Malomed, Symmetry **11**, 388 (2019).
[16] P. Xu, T. S. Deng, W. Zheng, and H. Zhai, Phys. Rev. A **103**, L061302 (2021).
[17] G. L. Alfimov, P. G. Kevrekidis, V. V. Konotop, and M. Salerno, Phys. Rev. E **66**, 046608 (2002).
[18] J. A. Sanders, F. Verhulst, and J. Murdock, *Averaging Methods in Nonlinear Dynamical Systems*, Applied Mathematical Science (Springer, New York, 2007).
[19] In the inter-SOC case Ω is a diagonal while σ is off-diagonal. In this case the terms proportional to σ in the averaged equations will be similar to the ones in (12) but with the roles of σ and Ω interchanged.